Eur. Phys. J. A **26**, 429–439 (2005)
DOI 10.1140/epja/i2005-10187-x

THE EUROPEAN PHYSICAL JOURNAL A

Electromagnetic radiative corrections in parity-violating electron-proton scattering

J. Arvieux[1], B. Collin[1,a], H. Guler[1,b], M. Morlet[1], S. Niccolai[1,c], S. Ong[1,2], and J. Van de Wiele[1]

[1] Institut de Physique Nucléaire, IN2P3-CNRS, Université de Paris-Sud, F-91406 Orsay Cedex, France
[2] Picardie Jules Verne University, F-80000 Amiens, France

Received: 21 November 2005 / Revised version: 20 December 2005 /
Published online: 18 January 2006 –
Communicated by Th. Walcher

Abstract. QED radiative corrections have been calculated for leptonic and hadronic variables in parity-violating elastic *ep* scattering. For the first time, the calculation of the asymmetry in the elastic radiative tail is performed without the peaking-approximation assumption in hadronic variables configuration. This method has been validated in a comparison with the PVA4 data. It has been also used to evaluate the radiative corrections to the parity-violating asymmetry measured in the G^0 experiment. The results obtained are here presented.

PACS. 25.30.Bf Elastic electron scattering – 13.60.-r Photon and charged-lepton interactions with hadrons

1 Introduction

Elastic scattering of longitudinally polarized electrons is subject to parity violation through the interference between γ and Z^0 exchange. These experiments give access to the weak nucleon form factors (FF), which are the equivalent, in the weak sector, of the usual electromagnetic form factors G_E and G_M. The weak nucleon form factors are related, in turn, to the strange form factors G_E^s and G_M^s, which are the contributions of strange currents to the form factors (see [1] and the following review articles [2–5]). According to QCD, this strangeness contribution arises from the presence of $s\bar{s}$ pairs in the nucleon sea. Many experiments have been performed recently or are still running at Bates (SAMPLE [6–8]), Mainz (PV-A4 [9,10]) and Jefferson Lab (G^0 [11] and HAPPEX [12]).

Electromagnetic radiation produced from the emission of a real or virtual photon by the electron (incoming or outgoing) or by the target (before or after interaction), gives rises to a radiative tail which extends to very low energies (in theory, down to zero energy for the scattered electron). Since detectors have an experimental resolution and since cuts are used in the data analysis, the measured cross-section and asymmetry have to be corrected in order to be compared to theoretical models. The first calculations applied to elastic *ep* scattering were done by Tsai [13], followed by a series of review papers [14–16]. This formalism has been later extended to scattering of polarized electrons [17]. All these calculations were done for experiments in which the scattered electron is detected, which was the case of SAMPLE, PV-A4, HAPPEX or G^0 at backward angles [18]. The originality of the G^0 experiment at forward angles was the detection of recoil protons. In this case, some of the approximations commonly used when scattered electrons are detected, such as the peaking approximation, are no more valid. Thanks to its large mass, radiative emission from the proton is negligible but the proton kinematics is affected by the radiative emission from the electron (angle, energy, Q^2).

QED radiative corrections have been calculated for hadronic kinematic variables in *ep* elastic scattering [19] and applied to recoil proton polarization. In this case, a method based on an electron structure-function representation, which is the analog of the Drell-Yann representation [20], was used. These calculations were applied to *ep* scattering experiments done at Jefferson Lab [21], aiming to determine the ratio of electric to magnetic proton form factors G_E^p/G_M^p at high momentum transfer as proposed by Akhiezer and Rekalo [22]. The classical method for computing corrections is based on the separation of the momentum phase space into hard- and soft-photons contributions to avoid infrared divergences [13].

[a] *Present address*: Department of Physics and Astronomy, Pennsylvania State University, PA 16802, USA.
[b] *Present address*: DESY, Hambourg, Germany.
[c] e-mail: silvia@jlab.org

This introduces a cutoff parameter which makes this method not easily applicable to construct an event operator. Bardin and Shumeiko [23] proposed a covariant cancellation method of infrared divergences which does not introduce additional parameters; however, a cutoff has still to be introduced for generating real radiated photons.

In the present work we calculate the corrections in both the leptonic and hadronic variables using an original method which is free of infrared divergences. Its interest is that it is exact and it can be integrated easily into numerical simulation programs such as GEANT. We then apply it to G^0 forward angles using the G^0-GEANT code [24]. Another original feature of the present calculation is the inclusion of Z^0 exchange, in addition to γ exchange, allowing to calculate the electroweak asymmetry of the radiative tail. We then calculate the corrected quantities of interest: integrated number of counts, time-of-flight (t.o.f.) spectra, Q^2 distributions. A full account of the present calculations is given in the thesis of Hayko Guler [25] (in French).

In sect. 2 we develop the formalism and define the Lagrangians, in sect. 3 we describe our method for avoiding divergences, in sect. 4 we describe briefly the G^0 apparatus and simulation method. The results are given in sect. 5 and we conclude in sect. 6.

2 Theoretical formalism for elastic scattering

The data analysis of parity-violating electron-nucleon scattering experiments involve the extraction of an asymmetry in the helicity-correlated cross-section. The raw data are first converted into an experimentally measured asymmetry (A_{exp}). That means that the false asymmetry due to helicity-correlated fluctuations in intensity, energy, positions and angles of the electron beam have already been taken into account. We assume also that background subtraction has already been done.

The asymmetry is commonly defined as

$$A = \frac{\left(\frac{\mathrm{d}\sigma}{\mathrm{d}\Omega}\right)^{+} - \left(\frac{\mathrm{d}\sigma}{\mathrm{d}\Omega}\right)^{-}}{\left(\frac{\mathrm{d}\sigma}{\mathrm{d}\Omega}\right)^{+} + \left(\frac{\mathrm{d}\sigma}{\mathrm{d}\Omega}\right)^{-}}\,, \tag{1}$$

where $\left(\frac{\mathrm{d}\sigma}{\mathrm{d}\Omega}\right)^{+}$ and $\left(\frac{\mathrm{d}\sigma}{\mathrm{d}\Omega}\right)^{-}$ are the cross-sections associated with incident electrons having helicity plus and minus, respectively. The plus (minus) helicity corresponds to the spin of the electron being aligned and in the same direction as (opposite to) its momentum. Calculation of the cross-section requires the knowledge of the amplitudes which are derived from the currents in the Feynman formalism.

The elastic-scattering amplitude has two components corresponding to the electromagnetic part $\mathcal{M}_\gamma$ and to the weak part $\mathcal{M}_Z$

$$\mathcal{M}\left(k', p', h_{e'}, h_{p'}, k, p, h_e, h_p\right) = \sum_{i=\gamma,Z} \mathcal{M}_i\left(k', p', h_{e'}, h_{p'}, k, p, h_e, h_p\right)\,, \tag{2}$$

where k and k' are the incident and scattered electron, p and p' are the incident and recoil proton momentum, respectively. h_e, h_p and $h_{e'}, h_{p'}$ are the electron and proton helicity in the initial and final state.

$$\mathcal{M}_\gamma = -ie^2 \frac{1}{q^2} J^P_{\nu\ em}\ j^\nu_{em}\,, \tag{3}$$

where j^ν_{em} is the Dirac leptonic electromagnetic current:

$$j^\nu_{em} = \bar{u}(k', h_{e'})\gamma^\nu u(k, h_e)\,, \tag{4}$$

and $J^P_{\nu\ em}$ is the hadronic part of the electromagnetic current. The weak amplitude is given by:

$$\mathcal{M}_Z = -i\frac{G}{2\sqrt{2}}\ \frac{1}{1 - q^2/{M_Z}^2} \left\{ \left(J^P_{\nu\ nc} + J^P_{\nu\ nc5}\right) j^\nu_{weak} - \left(J^{P^\nu}_{nc} + J^{P^\nu}_{nc5}\right)\ \frac{q_\nu q_\mu}{{M_Z}^2}\ j^\mu_{weak} \right\} \tag{5}$$

and the weak currents are obtained from

$$j^\mu_V = g^e_V\ \bar{u}(k', h_{e'})\ \gamma^\mu\ u(k, h_e)\,, \tag{6}$$

$$j^\mu_A = g^e_A\ \bar{u}(k', h_{e'})\ \gamma^\mu\gamma^5\ u(k, h_e)\,, \tag{7}$$

$$j^\mu_{weak} = j^\mu_V + j^\mu_A\,, \tag{8}$$

where G is the Fermi constant, g^e_V and g^e_A are the weak vector and axial charges, respectively. For electron scattering and at tree level they reduce to $g^e_V = -1 + 4\sin^2\theta_W$ and $g^e_A = 1$, respectively.

$J^P_{\nu\ nc}$ and $J^P_{\nu\ nc5}$ are the hadronic weak currents. The hadronic structure is parametrized in terms of form factors:

$$J^{EM\mu} = \langle x'|\hat{J}^{EM\mu}|x\rangle \tag{9}$$

$$= \overline{u}_{x'}\left[F^x_1(Q^2)\gamma^\mu + i\frac{F^x_2(Q^2)}{2M}\sigma^{\mu\nu}q_\nu\right]\ u_x\,, \tag{10}$$

$$J^{NC\mu} = \langle x'|\hat{J}^{NC\mu}|x\rangle \tag{11}$$

$$= \overline{u}_{x'}\left[\widetilde{F}^x_1(Q^2)\gamma^\mu + i\frac{\widetilde{F}^x_2(Q^2)}{2M}\sigma^{\mu\nu}q_\nu\right]\ u_x\,, \tag{12}$$

$$J^{NC\mu5} = \langle x'|\hat{J}^{NC\mu5}|x\rangle \tag{13}$$

$$= \overline{u}_{x'}\left[\widetilde{G}^x_A(Q^2)\gamma^\mu + i\frac{\widetilde{G}^x_P(Q^2)}{M}q^\mu\right]\gamma^5\ u_x\,, \tag{14}$$

where $x = p, n$ represents a proton p or a neutron n and u_x and $\overline{u}_{x'}$ are the Dirac spinors for the nucleon in the entrance and exit channel, respectively. F^x_1 and F^x_2 are

the electromagnetic form factors, $\widetilde{F}_1^x$ and $\widetilde{F}_2^x$ are the neutral weak vector form factors and $\widetilde{G}_A^x$ and $\widetilde{G}_P^x$ are, respectively, the axial and pseudo-scalar form factors. The latter enters in the cross-section and asymmetry through a $\mathcal{M}_Z$ squared term which is totally negligible.

The observables are usually expressed in terms of the Sachs form factors G_E^x, G_M^x, $\widetilde{G}_E^x$ and $\widetilde{G}_M^x$ rather than the Fermi and Dirac form factors F_1^x, F_2^x, $\widetilde{F}_1^x$, $\widetilde{F}_2^x$:

$$G_E^x(Q^2) = F_1^x(Q^2) - \tau F_2^x(Q^2)\,, \tag{15}$$
$$G_M^x(Q^2) = F_1^x(Q^2) + F_2^x(Q^2)\,,$$
$$\widetilde{G}_E^x(Q^2) = \widetilde{F}_1^x(Q^2) - \tau \widetilde{F}_2^x(Q^2)\,, \tag{16}$$
$$\widetilde{G}_M^x(Q^2) = \widetilde{F}_1^x(Q^2) + \widetilde{F}_2^x(Q^2)\,,$$

where $\tau = \frac{Q^2}{4{M_p}^2}$ is a kinematic factor and M_p is the proton mass.

The helicity-correlated cross-section is given by

$$\frac{\mathrm{d}^2\sigma_{h_e}}{\mathrm{d}\Omega_{e'}} = \frac{1}{16(2\pi)^2}\,\frac{|\boldsymbol{k}'|^2}{M\,|\boldsymbol{k}|} \times\frac{1}{2}\,\frac{\sum' |\mathcal{M}|^2}{\left|E_{p'}|\boldsymbol{k}'| + E_{e'}(|\boldsymbol{k}'| - |\boldsymbol{k}|\cos(\theta_{e'}))\right|}\,, \tag{17}$$

where the summation $\sum'$ is performed over all the spin variables except the incident electron helicity. The asymmetry can then be calculated from eq. (1):

$$A_{LR}(\boldsymbol{e}N) = -\frac{G_F Q^2}{4\pi\alpha\sqrt{2}}\frac{1}{\varepsilon(G_E^x)^2 + \tau(G_M^x)^2} \times\left\{\varepsilon\, G_E^x\, \widetilde{G}_E^x + \tau\, G_M^x\, \widetilde{G}_M^x - (1 - 4\sin^2\theta_W)\,\varepsilon'\, G_M^x\, \widetilde{G}_A^x\right\} \tag{18}$$

in which the Q^2 -dependence has been omitted for clarity of notation. ϵ, ϵ' are kinematic factors given by

$$\epsilon = \frac{1}{1 + 2(1+\tau)\tan^2\frac{\theta_{e'}}{2}}\,, \tag{19}$$
$$\epsilon' = \sqrt{\tau(1+\tau)(1-\epsilon^2)}\,, \tag{20}$$

$\theta_{e'}$ is the electron scattering angle and θ_W is the Weinberg angle.

The ultimate purpose of these experiments being to determine the strange content of the nucleon, one must isolate the contribution of the s-quark in the nucleon form factors. In order to do that, we decompose the electromagnetic, neutral and axial currents according to the different flavor contributions $f = u, d, s$:

$$\langle x'|\bar{u}_f\gamma_\mu u_f|x\rangle \equiv \tag{21}$$
$$\overline{u}_{x'}\left(F_1^{f,x}(Q^2)\gamma_\mu + i\frac{F_2^{f,x}(Q^2)}{2M}\sigma_{\mu\nu}q^\nu\right)u_x\,, \tag{22}$$
$$\langle x'|\bar{u}_f\gamma_\mu\gamma_5 u_f|x\rangle \equiv \tag{23}$$
$$\overline{u}_{x'}\left(\widetilde{G}_A^{f,x}(Q^2)\gamma_\mu + i\frac{\widetilde{G}_P^{f,x}(Q^2)}{M}q_\mu\right)\gamma_5\, u_x\,, \tag{24}$$

where u_f and $\bar{u}_f$ are the quarks fields. The pseudo-scalar form factors $\widetilde{G}_P^{f,x}$ being ignored, there are 18 form factors to be evaluated: 9 for the proton and 9 for the neutron. In order to reduce that number one uses charge symmetry, assuming that the p and the n are members of a perfect isospin doublet. Omitting the Q^2-dependence for clarity:

$$\begin{aligned} F_1^u &\equiv F_1^{u,p} = F_1^{d,n}, & F_2^u &\equiv F_2^{u,p} = F_2^{d,n},\\ F_1^d &\equiv F_1^{d,p} = F_1^{u,n}, & F_2^d &\equiv F_2^{d,p} = F_2^{u,n},\\ F_1^s &\equiv F_1^{s,p} = F_1^{s,n}, & F_2^s &\equiv F_2^{s,p} = F_2^{s,n}, \end{aligned} \tag{25}$$

$$\begin{aligned} G_A^u &\equiv \widetilde{G}_A^{u,p} = \widetilde{G}_A^{d,n},\\ G_A^d &\equiv \widetilde{G}_A^{d,p} = \widetilde{G}_A^{u,n},\\ G_A^s &\equiv \widetilde{G}_A^{s,p} = \widetilde{G}_A^{s,n}, \end{aligned}$$

After combining eqs. (15), (16) and eq. (25), the tree-level asymmetry can be finally expressed in terms of the electromagnetic, axial and strange nucleon form factors [26]:

$$\begin{aligned} A_{LR}(\boldsymbol{e}p) = -\frac{G_F Q^2}{4\pi\alpha\sqrt{2}}\Bigg\{&(1 - 4\sin^2\theta_W)\\ &-\frac{\varepsilon G_E^p G_E^n + \tau G_M^p G_M^n}{\varepsilon(G_E^p)^2 + \tau(G_M^p)^2}\Bigg\}\\ &+\frac{G_F Q^2}{4\pi\alpha\sqrt{2}}\frac{\varepsilon G_E^p}{\varepsilon(G_E^p)^2 + \tau(G_M^p)^2}\,G_E^s\\ &+\frac{G_F Q^2}{4\pi\alpha\sqrt{2}}\frac{\tau G_M^p}{\varepsilon(G_E^p)^2 + \tau(G_M^p)^2}\,G_M^s\\ &+\frac{G_F Q^2}{4\pi\alpha\sqrt{2}}\;\frac{(1 - 4\sin^2\theta_W)\,\varepsilon' G_M^p}{\varepsilon(G_E^p)^2 + \tau(G_M^p)^2}\;\widetilde{G}_A^p\,. \end{aligned} \tag{26}$$

The basic parameters entering in the formula at tree level are α, G_F and $\sin^2\theta_W$. They are known to 10^{-4} or better. Higher-order electroweak radiative corrections introduce correction parameters R_V^p and R_V^n which can be computed from the Standard Model [27]. The full (including higher-order corrections) asymmetry becomes

$$\begin{aligned} A_{LR}(\boldsymbol{e}p) = -\frac{G_F Q^2}{4\pi\alpha\sqrt{2}}\Bigg\{&(1 - 4\sin^2\theta_W)(1 + R_V^p)\\ &-(1 + R_V^n)\frac{\varepsilon G_E^p G_E^n + \tau G_M^p G_M^n}{\varepsilon(G_E^p)^2 + \tau(G_M^p)^2}\Bigg\}\\ &+\frac{G_F Q^2}{4\pi\alpha\sqrt{2}}(1 + R_V^{(0)})\frac{\varepsilon G_E^p}{\varepsilon(G_E^p)^2 + \tau(G_M^p)^2}\,G_E^s\\ &+\frac{G_F Q^2}{4\pi\alpha\sqrt{2}}\;(1 + R_V^{(0)})\frac{\tau G_M^p}{\varepsilon(G_E^p)^2 + \tau(G_M^p)^2}\,G_M^s\\ &+\frac{G_F Q^2}{4\pi\alpha\sqrt{2}}\;\frac{(1 - 4\sin^2\theta_W)\,\varepsilon' G_M^p}{\varepsilon(G_E^p)^2 + \tau(G_M^p)^2}\;\widetilde{G}_A^p\,. \end{aligned} \tag{27}$$

When recoil protons are detected instead of scattered electrons, the helicity-correlated cross-section becomes

$$\frac{\mathrm{d}^2\sigma_{h_e}}{\mathrm{d}\Omega_{p'}} = \frac{1}{16(2\pi)^2}\,\frac{|\boldsymbol{p}'|^2}{M\,|\boldsymbol{k}|} \times\frac{1}{2}\,\frac{\sum' |\mathcal{M}|^2}{\left|E_{e'}|\boldsymbol{p}'| + E_{p'}(|\boldsymbol{p}'| - |\boldsymbol{k}|\cos(\theta_{p'}))\right|}\,. \quad (28)$$

The asymmetry calculation follows the same steps as for scattered-electron detection.

3 QED radiative corrections

3.1 Parity-violating experiment representation in leptonic variables

The aim of the procedure is to get a differential cross-section $\mathrm{d}^3\sigma/\mathrm{d}\Omega_{e'}\mathrm{d}E_{e'}$ without any singularity in the full electron spectrum. We divide the scattered-electron energy interval into two regions. The first one, $E_{e'\,min} \le E_{e'} \le E_{e'\,cut}$ where $E_{e'\,cut} \equiv E_{e'\,elas} - \Delta E_{e'}$ corresponds to "hard photons" with a minimum energy $E_{e'\,min}$ which may be of the order of few MeV. The second one is defined by $E_{e'\,cut} \le E_{e'} \le E_{e'\,elas}$ which corresponds to the "soft-photon" region. The maximum energy of the outgoing electron corresponds to the elastic peak and is denoted by $E_{e'\,elas}$. The first requirement is that the integral

$$\int_{E_{e'\,min}}^{E_{e'\,elas}} \frac{\mathrm{d}^3\sigma}{\mathrm{d}\Omega_{e'}\mathrm{d}E_{e'}}\,\mathrm{d}E_{e'} = \int_{E_{e'\,min}}^{E_{e'\,cut}} \frac{\mathrm{d}^3\sigma}{\mathrm{d}\Omega_{e'}\mathrm{d}E_{e'}}\,\mathrm{d}E_{e'} + \int_{E_{e'\,cut}}^{E_{e'\,elas}} \frac{\mathrm{d}^3\sigma}{\mathrm{d}\Omega_{e'}\mathrm{d}E_{e'}}\,\mathrm{d}E_{e'} \quad (29)$$

should be as much as possible independent of the cutoff energy $\Delta E_{e'}$.

The three-dimensional differential cross-section which appears in the first term in the right-hand side of (29) is obtained from the five-dimensional differential cross-section:

$$\frac{\mathrm{d}^3\sigma}{\mathrm{d}\Omega_{e'}\mathrm{d}E_{e'}} = \int \frac{\mathrm{d}^5\sigma}{\mathrm{d}\Omega_{e'}\mathrm{d}E_{e'}\mathrm{d}\Omega_\gamma}\,\mathrm{d}\Omega_\gamma \quad (30)$$

corresponding to the bremsstrahlung process $e + p \to e + p + \gamma$. The two Feynman diagrams describing this process are displayed in fig. 1. The integral defined in (30) may be calculated in the peaking approximation when the scattering angle of the detected electron is not too small, which is the case for most experiments. In particular, this approximation is very good for the PV-A4 experiment at forward angles ($30^\circ \le \theta \le 40^\circ$) and for the PV-A4 and G^0 experiments at backward angles. The final result is found

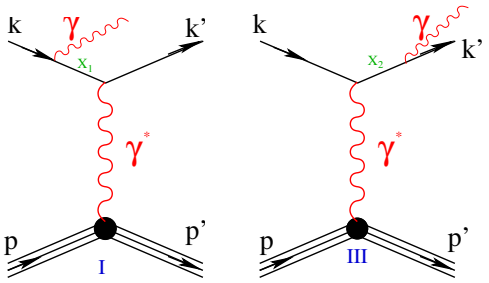

Fig. 1. Real-photon emission in virtual-photon exchange.

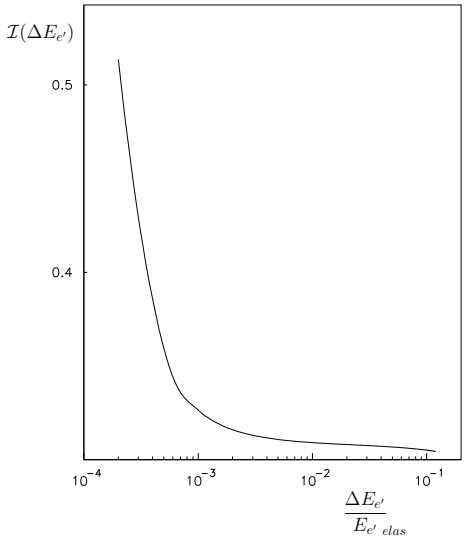

Fig. 2. Dependence of the right-hand side of eq. (29) with $\Delta E_{e'}$ in the A4 experiment: $E_e = 0.855$ GeV, $\theta_{e'} = 35^\circ$.

to be [14,28]:

$$\frac{\mathrm{d}^3\sigma}{\mathrm{d}\Omega_{e'}\mathrm{d}E_{e'}} \approx \left[\frac{\mathrm{d}^3\sigma}{\mathrm{d}\Omega_{e'}\mathrm{d}E_{e'}}\right]_{peaking} = \mathcal{K}_s\frac{\mathrm{d}^2\sigma_0(E_{e\,s}, Q_s^2)}{\mathrm{d}\Omega_{e'}} + \mathcal{K}_p\frac{\mathrm{d}^2\sigma_0(E_e, Q_p^2)}{\mathrm{d}\Omega_{e'}}, \quad (31)$$

where the index 0 stands for the Born elastic differential cross-section. The term with the s (respectively p) index represents the contribution of the left (right) Feynman diagram of fig. 1. The coefficients $\mathcal{K}_s$ and $\mathcal{K}_p$ are kinematic factors.

The second term in the right-hand side of (29) is usually expressed as

$$\int_{E_{e'\,cut}}^{E_{e'\,elas}} \frac{\mathrm{d}^3\sigma}{\mathrm{d}\Omega_{e'}\mathrm{d}E_{e'}}\,\mathrm{d}E_{e'} = \Big(1 + \delta(\Delta E_{e'})\Big)\,\frac{\mathrm{d}^2\sigma_0(E_e, Q^2)}{\mathrm{d}\Omega_{e'}}, \quad (32)$$

where the theoretical expression of $\delta(\Delta E_{e'})$ is given in [14, 28]. The numerical calculation of the right-hand side of eq. (29) is shown in fig. 2 for the PV-A4 parity-violating

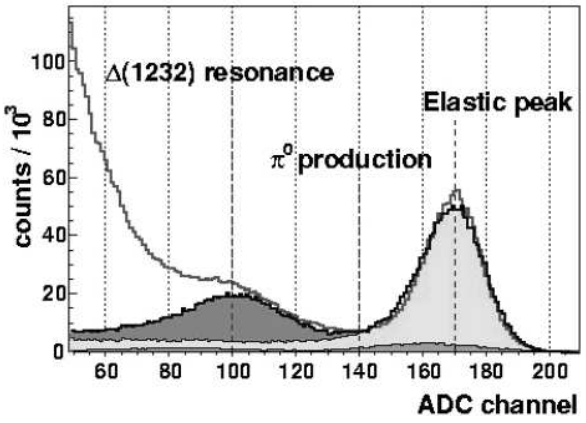

Fig. 3. Comparison of the experimental (solid line) and simulated spectra (filled grey areas) for the PV-A4 experiment [30]. The light-grey area corresponds to the simulated elastic *ep* scattering plus radiative corrections.

experiment. The minimum value of $\Delta E_{e'}$ in this kinematics is about 2 MeV.

An analytic expression for the three-dimensional differential cross-section in the energy range $E_{e'\,cut} \leq E_{e'} \leq E_{e'\,elas}$ can be defined as

$$\Big(\frac{\mathrm{d}^3\sigma}{\mathrm{d}\Omega_{e'}\mathrm{d}E_{e'}}\Big)_{anal} = a_0(\theta_{e'}) + a_1(\theta_{e'})\,E_{e'} + a_2(\theta_{e'})\,E_{e'}^2\,. \tag{33}$$

The three parameters a_0, a_1 and a_2 are fixed using the three conditions:

i) at $E_{e'} = E_{e'\,cut}$:

$$\Big[\frac{\mathrm{d}^3\sigma}{\mathrm{d}\Omega_{e'}\mathrm{d}E_{e'}}\Big]_{peaking} = \Big(\frac{\mathrm{d}^3\sigma}{\mathrm{d}\Omega_{e'}\mathrm{d}E_{e'}}\Big)_{anal}\,, \tag{34}$$

ii) at $E_{e'} = E_{e'\,cut}$:

$$\frac{\partial}{\partial E_{e'}}\Big[\frac{\mathrm{d}^3\sigma}{\mathrm{d}\Omega_{e'}\mathrm{d}E_{e'}}\Big]_{peaking} = \frac{\partial}{\partial E_{e'}}\Big(\frac{\mathrm{d}^3\sigma}{\mathrm{d}\Omega_{e'}\mathrm{d}E_{e'}}\Big)_{anal}, \tag{35}$$

iii) $$\int_{E_{e'\,cut}}^{E_{e'\,elas}} \Big(\frac{\mathrm{d}^3\sigma}{\mathrm{d}\Omega_{e'}\mathrm{d}E_{e'}}\Big)_{anal}\,\mathrm{d}E_{e'} = \Big(1+\delta(\Delta E_{e'})\Big) \times \frac{\mathrm{d}^2\sigma_0(E_e,Q^2)}{\mathrm{d}\Omega_{e'}}\,. \tag{36}$$

Full simulations performed with the Monte Carlo method and the experimental setup in the angular range between $40^\circ \leq \theta^\circ \leq 30$ at $E_e = 0.855$ GeV [29,30] have shown that the final spectrum is, within the experimental resolution, independent of the cutoff parameter $\Delta E_{e'}$ when its value is increased by a factor 2 to 4. The good agreement between the model and the PV-A4 experiment can be seen in fig. 3.

The simulated parity-violating asymmetry is then defined as

$$A = \begin{cases} A_{elas}, & E_{e'\,cut} \leq E_{e'} \leq E_{e'\,elas}, \\ \dfrac{\mathcal{K}_s\sigma_s A_s + \mathcal{K}_p\sigma_p A_p}{\mathcal{K}_s\sigma_s + \mathcal{K}_p\sigma_p}, & E_{e'\,min} \leq E_{e'} \leq E_{e'\,cut}, \end{cases} \tag{37}$$

where $\sigma_i \equiv \mathrm{d}^2\sigma_0(E_{e,s}, Q_i^2)/\mathrm{d}\Omega_{e'}$, $i = s, p$. The asymmetries A_s and A_p are the Born asymmetries calculated for the kinematics of the s and p channels through the relations given in the previous section.

3.2 Parity-violating experiment in proton variables

We describe here the method developed to take into account the internal radiative corrections when the proton, instead of the electron, is detected. Again, we will obtain for the proton spectrum a differential cross-section $\mathrm{d}^3\sigma/\mathrm{d}\Omega_{p'}\mathrm{d}E_{p'}$ without any singularity. The extension of the method derived for the electrons will give also the parity-violating asymmetry in the proton channel. As in the electron case, we define $E_{p'\,cut} \equiv E_{p'\,elas} - \Delta E_{p'}$ and we require the integral $\boldsymbol{\mathcal{I}}(\Delta E_{p'})$

$$\int_{E_{p'\,min}}^{E_{p'\,elas}} \frac{\mathrm{d}^3\sigma}{\mathrm{d}\Omega_{p'}\mathrm{d}E_{p'}}\,\mathrm{d}E_{p'} = \int_{E_{p'\,min}}^{E_{p'\,cut}} \frac{\mathrm{d}^3\sigma}{\mathrm{d}\Omega_{p'}\mathrm{d}E_{p'}}\,\mathrm{d}E_{p'} + \int_{E_{p'\,cut}}^{E_{p'\,elas}} \frac{\mathrm{d}^3\sigma}{\mathrm{d}\Omega_{p'}\mathrm{d}E_{p'}}\,\mathrm{d}E_{p'} \tag{38}$$

to be as much as possible independent of the energy cutoff $\Delta E_{p'}$. We have to modify the method of the previous section for two reasons. First, as we detect the proton, the differential cross-section is now given by

$$\frac{\mathrm{d}^3\sigma}{\mathrm{d}\Omega_{p'}\mathrm{d}E_{p'}} = \int \frac{\mathrm{d}^5\sigma}{\mathrm{d}\Omega_{p'}\mathrm{d}E_{p'}\mathrm{d}\Omega_\gamma}\,\mathrm{d}\Omega_\gamma\,. \tag{39}$$

Very forward angles of the outgoing electrons are allowed when the integration over all the directions of the photon is performed, so the cross-section has to be calculated at the amplitude level to be sure that gauge invariance is respected. Secondly, as we are interested to correct the experimental asymmetry from the internal radiative contribution, we need to introduce two more Feynman diagrams in the calculation, as shown in fig. 4.

The amplitude of the reaction $e + p \rightarrow e + p + \gamma$ is written as

$$\mathcal{M}\,(k', p', h_{e'}, h_{p'}, p_\gamma, h_\gamma, k, p, h_e, h_p) = \sum_{i=\mathrm{I},\cdots,\mathrm{IV}} \mathcal{M}_i\,(k', p', h_{e'}, h_{p'}, p_\gamma, h_\gamma, k, p, h_e, h_p)\,. \tag{40}$$

The four-vectors of the exchanged photon and Z^0 propagators are expressed in terms of the kinematic variables:

$$q = k - k' - p_\gamma = p' - p\,, \tag{41}$$

$$x_1 = k - p_\gamma\,, \qquad x_2 = k' + p_\gamma = k + p - p'\,. \tag{42}$$

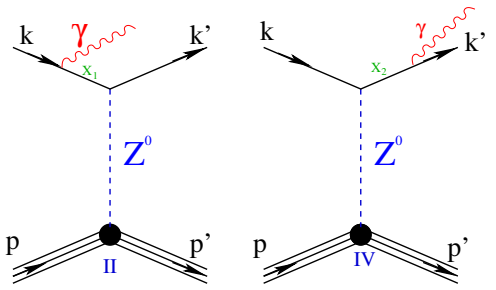

Fig. 4. Real-photon emission in virtual-Z^0 exchange.

The amplitudes I and III due to the exchanged photon with the propagator $-ig_{\nu\nu'}/q^2$ have one term:

$$\mathcal{M}_{\rm I} = ie^3 \frac{1}{x_1^2 - m_e^2} \frac{1}{q^2} J^P_{\nu\, em}\, T^{\nu\mu}_{{\rm I}\, em}\, \varepsilon^\star_\mu(p_\gamma, h_\gamma)\,, \quad (43)$$

$$T^{\nu\mu}_{{\rm I}\, em} = \bar{u}(k', h_{e'})\, \gamma^\nu\, (\not{x}_1 + m_e)\gamma^\mu\, u(k, h_e)\,, \quad (44)$$

$$\mathcal{M}_{\rm III} = ie^3 \frac{1}{x_2^2 - m_e^2} \frac{1}{q^2} J^P_{\nu\, em}\, T^{\mu\nu}_{{\rm III}\, em}\, \varepsilon^\star_\mu(p_\gamma, h_\gamma), \quad (45)$$

$$T^{\mu\nu}_{{\rm III}\, em} = \bar{u}(k', h_{e'})\, \gamma^\mu\, (\not{x}_2 + m_e)\gamma^\nu\, u(k, h_e)\,, \quad (46)$$

while the amplitudes II and IV due to the exchange of the Z^0 with the propagator $i(-g_{\nu\nu'} + q_\nu q_{\nu'}/{M_Z}^2)/(q^2 - {M_Z}^2)$ have each two different contributions:

$$\mathcal{M}_{\rm II} = ie \frac{G}{2\sqrt{2}} \frac{1}{x_1^2 - m_e^2} \frac{1}{1 - q^2/M_Z^2} \times \Big\{ \Big(J^P_{\nu\, nc} + J^P_{\nu\, nc5} \Big)\, T^{\nu\mu}_{\rm II}\, \varepsilon^\star_\mu(p_\gamma, h_\gamma) - \Big(J^{P\nu'}_{nc} + J^{P\nu'}_{nc5} \Big) \frac{q_\nu q_{\nu'}}{{M_Z}^2}\, T^{\nu\mu}_{\rm II}\, \varepsilon^\star_\mu(p_\gamma, h_\gamma) \Big\}, \quad (47)$$

$$T^{\nu\mu}_{{\rm II}\, V} = g^e_V\, \bar{u}(k', h_{e'})\, \gamma^\nu (\not{x}_1 + m_e)\gamma^\mu\, u(k, h_e), \quad (48)$$

$$T^{\nu\mu}_{{\rm II}\, A} = g^e_A\, \bar{u}(k', h_{e'})\, \gamma^\nu\gamma^5 (\not{x}_1 + m_e)\gamma^\mu\, u(k, h_e), \quad (49)$$

$$T^{\nu\mu}_{\rm II} = T^{\nu\mu}_{{\rm IV}\, V} + T^{\nu\mu}_{{\rm IV}\, A}, \quad (50)$$

$$\mathcal{M}_{\rm IV} = ie \frac{G}{2\sqrt{2}} \frac{1}{x_2^2 - m_e^2} \frac{1}{1 - q^2/M_Z^2} \times \Big\{ \Big(J^P_{\nu\, nc} + J^P_{\nu\, nc5} \Big)\, T^{\mu\nu}_{\rm IV}\, \varepsilon^\star_\mu(p_\gamma, h_\gamma) - \Big(J^{P\nu'}_{nc} + J^{P\nu'}_{nc5} \Big) \frac{q_\nu q_{\nu'}}{{M_Z}^2}\, T^{\mu\nu}_{\rm IV}\, \varepsilon^*_\mu(p_\gamma, h_\gamma) \Big\}, \quad (51)$$

$$T^{\mu\nu}_{{\rm IV}\, V} = g^e_V\, \bar{u}(k', h_{e'})\, \gamma^\mu (\not{x}_2 + m_e)\gamma^\nu\, u(k, h_e), \quad (52)$$

$$T^{\mu\nu}_{{\rm IV}\, A} = g^e_A\, \bar{u}(k', h_{e'})\, \gamma^\mu (\not{x}_2 + m_e)\gamma^\nu\gamma^5\, u(k, h_e), \quad (53)$$

$$T^{\mu\nu}_{\rm IV} = T^{\mu\nu}_{{\rm IV}\, V} + T^{\mu\nu}_{{\rm IV}\, A}\,. \quad (54)$$

In the energy range where the parity-violating experiments are performed ($0.1 \le Q^2 \le 1$ (GeV/c)^2, terms proportional to $1/{M_Z}^2$ are neglected, therefore:

$$\mathcal{M}_{\rm II} \approx ie \frac{G}{2\sqrt{2}} \frac{1}{x_1^2 - m_e^2} \times \Big\{ \Big(J^P_{\nu\, nc} + J^P_{\nu\, nc5} \Big) \Big(T^{\nu\mu}_{{\rm II}\, V} + T^{\nu\mu}_{{\rm IV}\, A} \Big)\, \varepsilon^\star_\mu(p_\gamma, h_\gamma) \Big\}, \quad (55)$$

and

$$\mathcal{M}_{\rm IV} \approx ie \frac{G}{2\sqrt{2}} \frac{1}{x_2^2 - m_e^2} \times \Big\{ \Big(J^P_{\nu\, nc} + J^P_{\nu\, nc5} \Big) \Big(T^{\mu\nu}_{{\rm IV}\, V} + T^{\mu\nu}_{{\rm IV}\, A} \Big)\, \varepsilon^\star_\mu(p_\gamma, h_\gamma) \Big\}. \quad (56)$$

The total amplitude is the sum of two terms,

$$\mathcal{M} = \mathcal{M}^{PC} + \mathcal{M}^{PV}\,. \quad (57)$$

The interference of these two terms will produce the parity-violating asymmetry. The parity-conserving amplitude $\mathcal{M}^{PC}$ is due to photon exchange and it contains a part of the Z^0 exchange. The parity-violating amplitude $\mathcal{M}^{PV}$ is due to part of the Z^0 exchange contribution in the Feynman diagrams II and IV. Explicitly, this amplitude is

$$\mathcal{M}^{PV} = \mathcal{M}^{PV}_{\rm II} + \mathcal{M}^{PV}_{\rm IV}\,, \quad (58)$$

$$\mathcal{M}^{PV}_{\rm II} = ie \frac{G}{2\sqrt{2}} \frac{1}{x_1^2 - m_e^2} \times \Big(J^P_{\nu\, nc}\, T^{\nu\mu}_{{\rm II}\, A} + J^P_{\nu\, nc5}\, T^{\nu\mu}_{{\rm II}\, V} \Big)\, \varepsilon^\star_\mu(p_\gamma, h_\gamma), \quad (59)$$

$$\mathcal{M}^{PV}_{\rm IV} = ie \frac{G}{2\sqrt{2}} \frac{1}{x_2^2 - m_e^2} \times \Big(J^P_{\nu\, nc}\, T^{\mu\nu}_{{\rm IV}\, A} + J^P_{\nu\, nc5}\, T^{\mu\nu}_{{\rm IV}\, V} \Big)\, \varepsilon^*_\mu(p_\gamma, h_\gamma). \quad (60)$$

The differential cross-section is then calculated in the laboratory system in terms of the amplitudes by

$$\frac{{\rm d}^5\sigma}{{\rm d}\Omega_{p'}{\rm d}E_{p'}{\rm d}\Omega_\gamma} = \frac{1}{32(2\pi)^5} \frac{|\boldsymbol{p}'|E_\gamma}{M\,|\boldsymbol{k}|} \times \frac{1}{4} \frac{\sum |\mathcal{M}|^2}{|E_\gamma + E_{e'} + \boldsymbol{u}_\gamma \cdot (\boldsymbol{p}' - \boldsymbol{k})|}, \quad (61)$$

where the summation is performed over all the helicity states of the incoming electron, the target, the outgoing proton and the outgoing photon. The differential cross-section of the outgoing proton is then expressed as in (39), after integration over all the photon angles.

The parity-violating asymmetry is calculated in a similar way. First we calculate the differential cross-section as a function of the beam helicity $h_e = \pm 1/2$:

$$\frac{\mathrm{d}^5\sigma_{h_e}}{\mathrm{d}\Omega_{p'}\mathrm{d}E_{p'}\mathrm{d}\Omega_\gamma} = \frac{1}{32(2\pi)^5}\,\frac{|\boldsymbol{p}'|E_\gamma}{M\,|\boldsymbol{k}|} \times\frac{1}{2}\,\frac{\sum'|\mathcal{M}|^2}{|E_\gamma + E_{e'} + \boldsymbol{u}_\gamma\cdot(\boldsymbol{p}'-\boldsymbol{k})|}\,. \quad (62)$$

The prime index over the summation means that the sum is performed over all the spin variables except the incident electron helicity. The parity-violating asymmetry of the proton spectrum then reads

$$A = \left(\frac{\mathrm{d}^3\sigma_{1/2}}{\mathrm{d}\Omega_{p'}\mathrm{d}E_{p'}} - \frac{\mathrm{d}^3\sigma_{-1/2}}{\mathrm{d}\Omega_{p'}\mathrm{d}E_{p'}}\right)\Big/\left(\frac{\mathrm{d}^3\sigma_{1/2}}{\mathrm{d}\Omega_{p'}\mathrm{d}E_{p'}} + \frac{\mathrm{d}^3\sigma_{-1/2}}{\mathrm{d}\Omega_{p'}\mathrm{d}E_{p'}}\right) \quad (63)$$

with

$$\frac{\mathrm{d}^3\sigma_{h_e}}{\mathrm{d}\Omega_{p'}\mathrm{d}E_{p'}} = \int\frac{\mathrm{d}^5\sigma_{h_e}}{\mathrm{d}\Omega_{p'}\mathrm{d}E_{p'}\mathrm{d}\Omega_\gamma}\,\mathrm{d}\Omega_\gamma\,. \quad (64)$$

Now we are able to calculate the integral

$$\int_{E_{p'\,min}}^{E_{p'\,cut}}\frac{\mathrm{d}^3\sigma}{\mathrm{d}\Omega_{p'}\mathrm{d}E_{p'}}\,\mathrm{d}E_{p'} \quad (65)$$

for any value of $\Delta E_{p'} \neq 0$. As in the electron case, the integral in the energy range $E_{p'\,cut} \leq E_{p'} \leq E_{p'\,elas}$ is proportional to the Born elastic differential cross-section:

$$\int_{E_{p'\,cut}}^{E_{p'\,elas}}\frac{\mathrm{d}^3\sigma}{\mathrm{d}\Omega_{p'}\mathrm{d}E_{p'}}\,\mathrm{d}E_{p'} = \mathcal{A}(\Delta E_{p'})\,\frac{\mathrm{d}^2\sigma_0(E_e,Q^2)}{\mathrm{d}\Omega_{p'}}. \quad (66)$$

Its calculation is given by the following ratio:

$$\mathcal{A}(\Delta E_{p'}) = \left(\int\mathcal{K}(\Delta E_{p'})\,\frac{\mathrm{d}^5\sigma}{\mathrm{d}\Omega_{p'}\mathrm{d}E_{p'}\mathrm{d}\Omega_\gamma}\,\mathrm{d}\Omega_\gamma\right) \Big/\left(\int\frac{\mathrm{d}^5\sigma}{\mathrm{d}\Omega_{p'}\mathrm{d}E_{p'}\mathrm{d}\Omega_\gamma}\,\mathrm{d}\Omega_\gamma\right) \quad (67)$$

with [31]

$$\mathcal{K}(\Delta E_{p'}) \equiv \frac{e^{\delta_{vertex}+\delta_R}}{(1-\delta_{vacuum}/2)^2}\,. \quad (68)$$

The meaning of $\mathcal{K}(\Delta E_{p'})$ is clear. For each value of $\theta_{p'}$, $\phi_{p'}$, $E_{p'}$, θ_γ and ϕ_γ, the value of $\Delta E_{p'}$ is equal to $E_{p'\,elas} - E_{p'}$. The three-body kinematics give the energy of the photon E_γ and the complete kinematics of the outgoing electron $\theta_{e'}$, $\phi_{e'}$ and $E_{e'}$ through the energy-momentum conservation. Comparison with the elastic-scattering $e + p \rightarrow e + p$ reaction at the same angle gives the value of $\Delta E_{e'} = E_{e'\,elas} - E_{e'}$. The ratio $\mathcal{K} = e^{\delta_{vertex}+\delta_R}/(1-\delta_{vacuum}/2)^2$ is the attenuation factor, which depends on $\Delta E_{e'}$, induced by the internal radiative correction on the electron side. It is a generalization to all orders of the $1 + \delta$ term of eq. (36) as can be seen if we make a Taylor expansion of $\mathcal{K}$. Finally the attenuation factor $\mathcal{A}(\Delta E_{p'})$ as defined in eq. (67) is the average attenuation factor when we integrate over all the directions of the photon. The explicit formulae used in the code to calculate δ_{vertex}, δ_R and δ_{vacuum} are taken from [31]:

$$\delta_R = \frac{\alpha}{\pi}\left\{\ln\left(\frac{(\Delta E_s)^2}{E_e E_{e'}}\right)\left[\ln\left(\frac{Q^2}{m_e^2}\right)-1\right] - \frac{1}{2}\ln^2\left(\frac{E_e}{E_{e'}}\right) + \frac{1}{2}\ln^2\left(\frac{Q^2}{m_e^2}\right) - \frac{\pi^2}{3} + Sp\Big(\cos^2(\theta_{e'}/2)\Big)\right\}, \quad (69)$$

$$\Delta E_s = \frac{E_e}{E_{e'\,elas}}(E_{e'\,elas} - E_{e'})\,, \quad (70)$$

$$\delta_{vacuum} = \frac{\alpha}{\pi}\frac{2}{3}\left\{-\frac{5}{3} + \ln\left(\frac{Q^2}{m_e^2}\right)\right\}, \quad (71)$$

$$\delta_{vertex} = \frac{\alpha}{\pi}\left\{\frac{3}{2}\ln\left(\frac{Q^2}{m_e^2}\right) - 2 - \frac{1}{2}\ln^2\left(\frac{Q^2}{m_e^2}\right) + \frac{\pi^2}{6}\right\}. \quad (72)$$

The value of the integral $\boldsymbol{\mathcal{I}}(\Delta E_{p'})$ as a function of $\Delta E_{p'}$ has been performed for $48^\circ \leq \theta_{p'} \leq 77^\circ$. It is plotted in fig. 5 for one scattering angle of the detected proton. The value of the cutoff parameter is chosen so that this integral reaches its minimum value.

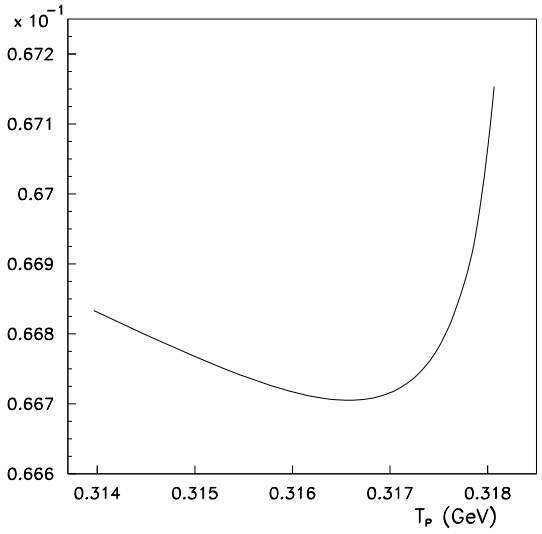

Fig. 5. $\boldsymbol{\mathcal{I}}(\Delta E_{p'})$ as a function of the kinetic energy of the detected proton for $\theta_{p'} = 60^\circ$.

As in the electron case, we assume that for the kinetic-energy range of the scattered proton $T_{p'\,elas} - \Delta E_{p'} \leq T_{p'} \leq T_{p'\,elas}$

$$\left(\frac{\mathrm{d}^3\sigma}{\mathrm{d}\Omega_{p'}\mathrm{d}E_{p'}}\right)_{anal} = a_0(\theta_{p'}) + a_1(\theta_{p'})\,(T_{p'} - T_{p'\,elas}) + a_2(\theta_{p'})\,(T_{p'} - T_{p'\,elas})^2\,. \quad (73)$$

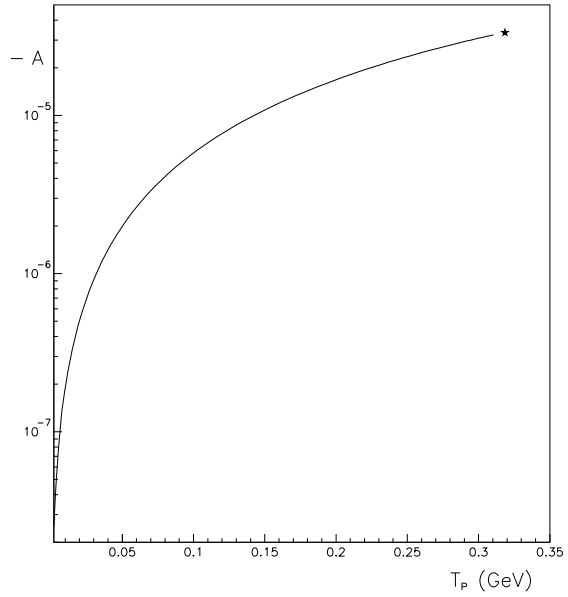

Fig. 6. Parity-violating asymmetry as a function of the kinetic energy of the detected proton for $\theta_{p'} = 60°$. The star $\star$ represents the Born asymmetry.

The determination of the three coefficients a_0, a_1 and a_2 is obtained by the following conditions:

i) at $E_{p'} = E_{p'\,cut}$:

$$\left(\frac{\mathrm{d}^3\sigma}{\mathrm{d}\Omega_{p'}\mathrm{d}E_{p'}}\right) = \left(\frac{\mathrm{d}^3\sigma}{\mathrm{d}\Omega_{p'}\mathrm{d}E_{p'}}\right)_{anal}, \tag{74}$$

ii) at $E_{p'} = E_{p'\,cut}$:

$$\frac{\partial}{\partial E_{p'}}\left(\frac{\mathrm{d}^3\sigma}{\mathrm{d}\Omega_{p'}\mathrm{d}E_{p'}}\right) = \frac{\partial}{\partial E_{p'}}\left(\frac{\mathrm{d}^3\sigma}{\mathrm{d}\Omega_{p'}\mathrm{d}E_{p'}}\right)_{anal}, \tag{75}$$

iii) $$\int_{E_{p'\,cut}}^{E_{p'\,elas}} \left(\frac{\mathrm{d}^3\sigma}{\mathrm{d}\Omega_{p'}\mathrm{d}E_{p'}}\right)_{anal} \mathrm{d}E_{p'} = \mathcal{A}(\Delta E_{p'}) \times \frac{\mathrm{d}^2\sigma_0(E_e, Q^2)}{\mathrm{d}\Omega_{p'}}. \tag{76}$$

The parity-violating asymmetry is calculated through the relation (63) for $E_{p'} \leq E_{p'\,cut}$ and near the elastic peak, its value is linearly interpolated between its value at $E_{p'} = E_{p'\,cut}$ and the Born asymmetry calculated at $E_{p'} = E_{p'\,elas}$. The variation of this asymmetry as a function of the kinetic energy of the scattered proton is plotted in fig. 6 for $\theta_{p'} = 60°$.

4 Application to the G^0 experiment at forward angles

The G^0 experiment [32], performed in Hall C at Jefferson Lab, measures the parity-violating elastic electron scattering from the nucleon. Asymmetries of the order of one part per million from scattering of a polarized electron beam are determined using a dedicated apparatus. It consists of specialized beam monitoring and control systems, a cryogenic hydrogen target and a superconducting, toroidal magnetic spectrometer equipped with plastic scintillation counters as well as fast readout electronics for the measurement of individual events. The polarized electrons scattered from a 20 cm liquid-hydrogen target; the recoiling elastic protons were detected in a spectrometer to allow simultaneous measurement of the wide range of momentum transfer $0.12 \leq Q^2 \leq 1.0$ (GeV/c)^2. The spectrometer included an eight-coil superconducting magnet and eight sets (or octants) of scintillating detectors. Four octants (numbered 1-3-5-7) and their associated electronics were built by the North-American (USA, Canada) part of the G^0 Collaboration and four octants (2-4-6-8) and their associated electronics were built by the French (IPN Orsay, LPSC Grenoble) part of the G^0 Collaboration. Each set consisted of 16 scintillator pairs used in coincidence to cover the range of momentum transfers (smallest detector number corresponding to the lowest momentum transfer). The scattering angle varies from 52 to 76 degrees, depending on the detector number. Because of the correlation between the momentum and scattering angle of the elastic protons (higher momentum corresponds to more forward proton scattering angles), detector 15 covered the range of momentum transfers between 0.44 and 0.88 (GeV/c)^2, which we divided into three bins having average momentum transfers of 0.51, 0.63 and 0.79 (GeV/c)^2. Custom time-encoding electronics sorted detector events by time of flight (t.o.f.); elastic protons arrived about 20 ns after the passage of the electron bunch through the target. A typical time-of-flight spectrum is shown in fig. 7. The final results of the G^0 forward-angle experiment are shown in [11].

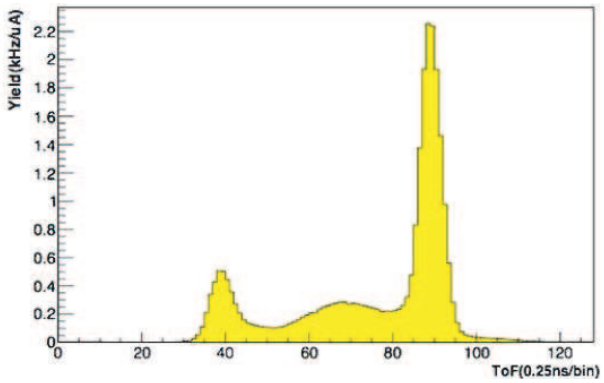

Fig. 7. Experimental yield as a function of t.o.f. for detector 8. The elastic protons correspond to the rightmost peak.

Radiative corrections for G^0 have been estimated in a simulation using the G0-GEANT package [24]. The electron can, in principle, lose all its energy through radiation, but the probability that it loses 500 MeV or less is 96%.

Moreover, 60% lose 1 keV or less. The few events for which the electron energy loss is more than 500 MeV correspond to protons having times of flight out of the G^0 experimental cuts, thus they are not considered in our calculation. Therefore, the GEANT simulations have been done in the energy interval $E_{inc} = 2.5$–3.0 GeV only and for recoil proton angle $\theta_{p'} = 48°$–$77°$ and energy $T_{p'} = 2\ \text{MeV} - T_{p'}^{el}$. The cross-sections have been interpolated for intermediate values using a spline method. In order to obtain rates, each event (number j) is normalized through a weight w_j proportional to the cross-section [33]:

$$w_j = \mathcal{L}\frac{\Delta\phi}{N_T}\frac{\mathrm{d}^3\sigma_j}{\mathrm{d}\Omega\mathrm{d}E}\sin\theta_j[\theta_{max}(E_j^{inc}) - \theta_{min}(E_j^{inc})] \times[E_{max}(E_j^{inc},\theta_j) - E_{min}(E_j^{inc},\theta_j)]\,, \quad (77)$$

where $\mathcal{L}$ is the luminosity, $\Delta\phi$ is the polar angle opening and N_T is the number of drawings. In the case of elastic scattering (Born term), the weight is simply given by

$$w_j = \mathcal{L}\frac{\Delta\theta\Delta\phi}{N_T}\sin\theta_j\frac{\mathrm{d}^2\sigma_j}{\mathrm{d}\Omega}.$$

5 Results

5.1 Time-of-flight spectra

Two calculations are performed without and with RC:

– In the first case, the t.o.f. of elastically scattered protons, without any energy loss nor radiative corrections is calculated. The width of the peak is essentially given by the experimental resolution as calculated by GEANT. The elastic peak is fitted with a Gaussian allowing to determine the position of the maximum, in order to define cuts within which the asymmetry is calculated. The resulting spectra are shown in fig. 8, where only detector 8, corresponding to the middle of the focal plane, is shown for reference. The only difference in the two spectra is a binning of 250 ps for the French (FR) electronics (top) and a binning of 1 ns for the North-American (NA) electronics (bottom).
– In the second case, the proton t.o.f. spectra are calculated after applying energy losses and full RC. The result obtained for detector 8 is shown as a solid line in fig. 9, overlaid to the pure elastic spectra (dash-dotted line).

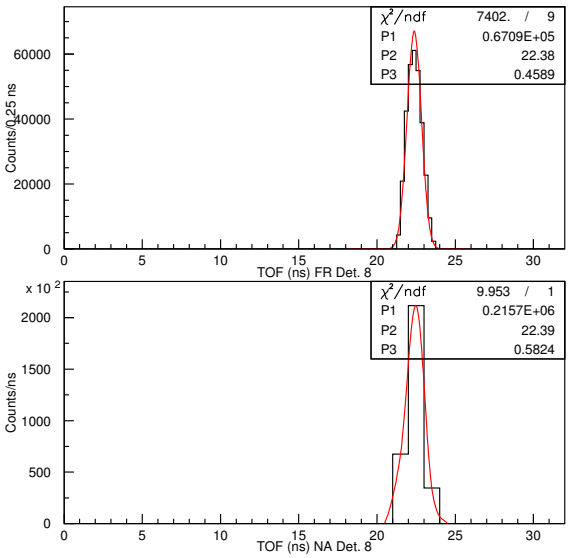

Fig. 8. Simulated elastic-proton time-of-flight distributions for Det. 8 (top: FR, bottom: NA). The Gaussian fits are performed to extract the position of the mean.

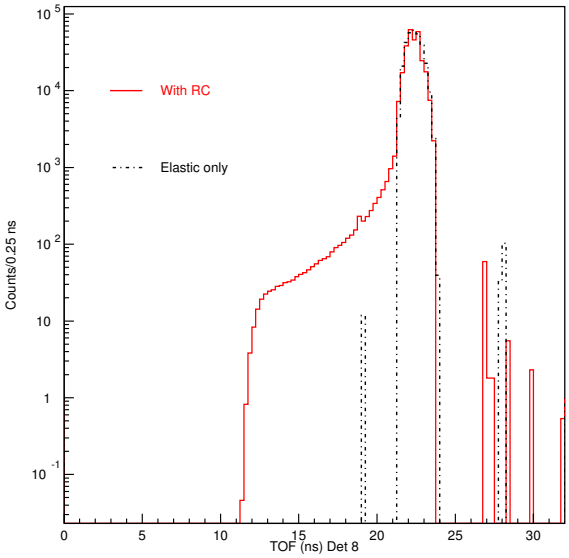

Fig. 9. Comparison of time-of-flight spectra (FR Det. 8) without (dash-dotted line) and with (solid line) radiative corrections.

5.2 Asymmetries

The asymmetry is calculated using eq. (26) with the following numerical values [3]:

$$\begin{aligned}\sin^2\theta_W &= 0.23117\,,\\ G_F &= 1.16639\times10^{-5}\ \text{GeV}^{-2}\,,\\ R_V^p &= -0.054\pm0.033\,,\\ R_V^n &= -0.0143\pm0.0004\,,\\ R_V^{(0)} &= 0.\end{aligned}$$

G_E^s and G_M^s are parametrized with a dipole form according to [3]. A discussion of the latest electromagnetic form factors can be found in [11]. The strangeness content parameters are from Hammer *et al.* [34] with $\mu_s = -0.24$ and $\rho_s = -2.93$. These values have been taken from a review paper by Kumar and Souder [2]. These parameters are used here only as an example of a strange asymmetry

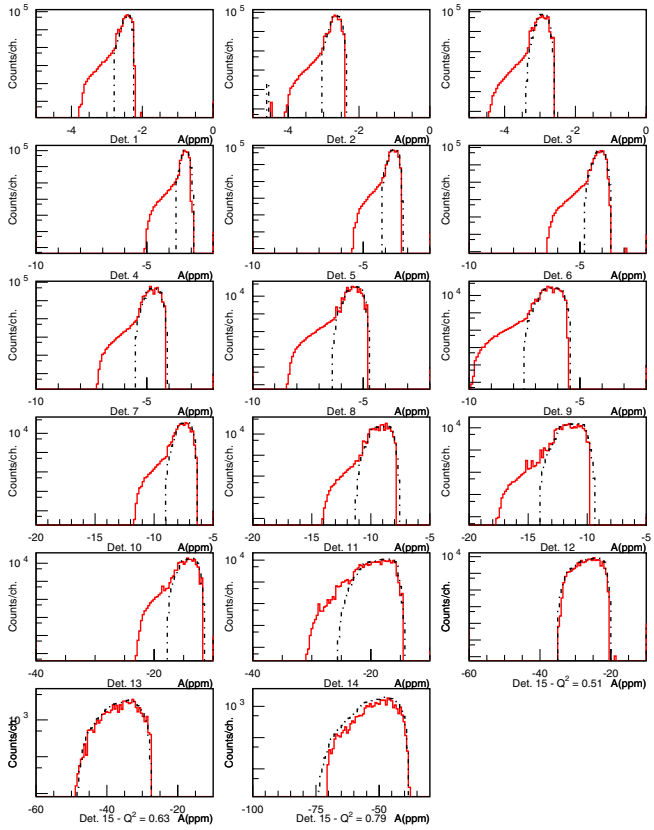

Fig. 10. Asymmetry distributions (in ppm), for each detector. The dash-dotted line represents the elastic case, the solid one the radiative case.

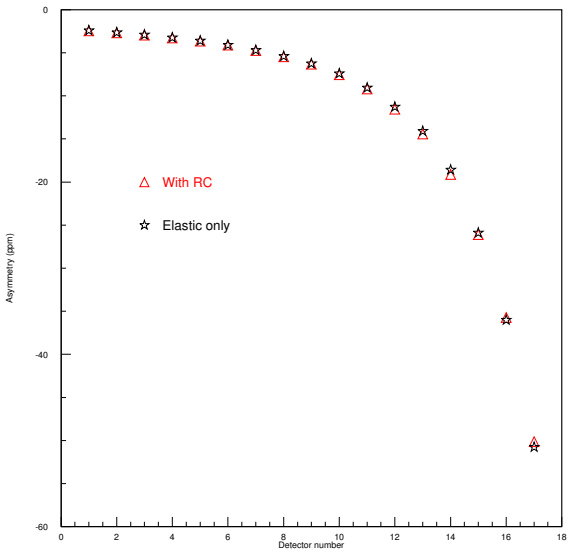

Fig. 11. Mean value of the asymmetry for each detector. The stars represent the elastic case, the triangles the radiative one. The "French cuts" on the t.o.f. distributions have been applied.

Table 1. Ratio of asymmetries A_{el}/A_{RC} as a function of the detector number where A_{el} is the elastic (Born term) asymmetry and A_{RC} is the asymmetry corrected for radiative emission.

Detector #	Ratio
1	0.9971380
2	0.9898130
3	0.9912670
4	0.9911590
5	0.9933250
6	0.9964800
7	0.9915390
8	0.9881630
9	0.9910010
10	0.9828710
11	0.9871740
12	0.9790010
13	0.9767610
14	0.9725560
15/1 $Q^2 = 0.51$	0.9922500
15/2 $Q^2 = 0.63$	1.008340
15/3 $Q^2 = 0.79$	1.012570

calculation. Electromagnetic radiative corrections are rather insensitive to the electroweak parameters. Detailed calculations are shown on the FR detectors spectra only. Figure 10 shows the asymmetry distribution without (dash-dotted line) and with RC (solid line). In the elastic case, the asymmetry reduces to the one calculated from the Born term only, and it can be compared directly to theoretical models.

The mean asymmetry value is plotted in fig. 11. The effect of radiative corrections is to increase the average asymmetry, following the increase in Q^2. The ratios between elastic and RC-corrected asymmetries are given in table 1.

The asymmetry increase is of the order of 0.5–1.0% for detectors 1–9, reaching 2.0 % for detector 12 and up to 3.0% for detector 14. These ratios should be almost independent of the model chosen and therefore valid for the no-strangeness value A_0. It is not clear if the dispersion of correction factors between 2 adjacent detectors (*e.g.* between Det. 8-9-10 or 10-11-12), which is of the order of 0.3%, is an indication of the present statistical/systematical errors or if it is a genuine effect due to differences in acceptance.

5.3 Uncertainty estimate

An error estimate is made based on the assumption that the elastic cuts have a 10% uncertainty. Therefore, the radiative corrections are calculated for cuts which are 5% larger than the elastic cuts (by increasing the upper limit by 2.5% and decreasing the lower limit by 2.5%) and 5% smaller than the elastic cuts (by decreasing the upper limit

by 2.5% and increasing the lower limit by 2.5%). Then we take the ratio of these two quantities for each detector. This should represent an upper limit of the radiative correction uncertainties since the elastic cuts are known to better than 10%. The corresponding uncertainty would vary slowly from 0.1% for Det. 1 to 0.5% for Det. 13, 1% for Det. 14 and between 0.0% and 0.7% for Det. 15, depending on the Q^2 cut. An alternative error estimate is obtained by making a global fit of the ratio A_{el}/A_{RC} with a polynomial and assuming that the difference with the actual RC correction is due to systematics: in that case the uncertainty is globally estimated to be of the order of 0.1–0.3% or 10% of the actual correction depending on detector number.

Another problem which has been investigated is the one of correction double counting. When the background under the elastic peak is removed by a pure fitting procedure, it also contains the RC tail contribution to the peak. Therefore, the corresponding elastic asymmetry should not be corrected for RC effects. In order to estimate the sensitivity of the RC corrections, at the border of the elastic peak, we have calculated them by adding or removing 1 ns from the elastic cuts. This effect has been estimated to be about 2% of the RC corrections which are themselves of the order of 2%, so that double counting can be neglected at first order.

6 Summary and conclusions

We have calculated the full electromagnetic radiative corrections for elastic *ep* scattering in leptonic or hadronic variables. A code has been constructed to extract the parity-violating asymmetry from the experimental measured asymmetry. The procedure is validated through a comparison between the simulation results and the data in the kinematic configuration of the PV-A4 experiment. Radiative corrections for the G^0 parity-violating elastic-scattering experiment have been estimated by feeding our model calculations through a Monte Carlo detector simulation. This code could also be used for the next asymmetry measurement in the backward-angle configuration of G^0.

The authors are grateful to the PV-A4 and G^0 Collaborations for their constructive remarks and support. The comments of Jiangliai Liu and Kaz Nakahara are particularly acknowledged.

References

1. D.B. Kaplan, A. Manohar, Nucl. Phys. B **310**, 527 (1988).
2. K.S. Kumar, P.A. Souder, Prog. Part. Nucl. Phys. **45**, S333 (2000).
3. M.J. Musolf *et al.*, Phys. Rep. **1**, 239 (1994).
4. D.H. Beck, B.R. Holstein, Int. J. Mod. Phys. E **10**, 1 (2001).
5. D.H. Beck, R.D. MacKeown, Annu. Rev. Nucl. Part. Sci. **51**, 189 (2001).
6. E.J. Beise, M.L. Pitt, D.T. Spayde, Prog. Part. Nucl. Phys. **54**, 289 (2005).
7. T. Ito *et al.*, Phys. Rev. Lett. **92**, 102003 (2004).
8. D.T. Spayde *et al.*, Phys. Lett. B **58**, 79 (2004).
9. F.E. Maas *et al.*, Phys. Rev. Lett. **93**, 022002 (2004).
10. F.E. Maas *et al.*, Phys. Rev. Lett. **94**, 082001 (2005).
11. D.S. Armstrong *et al.*, Phys. Rev. Lett. **95**, 092001 (2005).
12. K.A. Aniol *et al.*, Phys. Rev. C **69**, 065501 (2004).
13. Y.S Tsai, Phys. Rev. **122**, 1898 (1961).
14. L.W. Mo, Y.S. Tsai, Rev. Mod. Phys. **41**, 205 (1969).
15. L.C. Maximon, Rev. Mod. Phys. **41**, 193 (1969).
16. Y.S. Tsai, Rev. Mod. Phys. **46**, 815 (1974).
17. L.C. Maximon, W.C. Parke, Phys. Rev. C **61**, 045502 (2000).
18. Jefferson Lab Experimental proposal PR 05-108.
19. A.F. Afanasev *et al.*, Phys. Lett. B **514**, 269 (2001).
20. S. Drell, T.M. Yan, Phys. Rev. Lett. **25**, 316 (1970).
21. M.K. Jones *et al.*, Phys. Rev. Lett. **84**, 1398 (2000).
22. A.I. Akhiezer, M.P. Rekalo, Sov. J. Part. Nucl. **3**, 277 (1974).
23. D. Bardin, N. Shumeiko, Nucl. Phys. B **127**, 242 (1977).
24. L. Hannelius, private communication.
25. H. Guler, Thesis, Université Paris-Sud, December 2003.
26. J. Arvieux *et al.*, G^0-Collaboration internal report, `http://g0web.jlab.org/analysislog/Analysis_Notes/050711_100102/PV-short-110705.pdf`, July 2005.
27. S. Eidelman *et al.*, Phys. Lett. B **592**, 1109 (2004).
28. S. Ong, M.P. Rekalo, J. Van de Wiele, Eur. Phys. J. A **6**, 215 (1999).
29. B. Collin, Thesis, Université Paris-Sud, November 2002.
30. L. Capozza, Eur. Phys. J. A **24**, s02, 65 (2005) DOI: 10.1140/epjad/s2005-04-014-2.
31. M. Vanderhaegen *et al.*, Phys. Rev. C **62**, 025501 (2000).
32. P. Roos *et al.*, Eur. Phys. J. A **24**, 59 (2005); to be submitted to Nucl. Instrum. Methods.
33. J. Van de Wiele, M. Morlet, Eur. Phys. J. A **24**, s02, 137 (2005) DOI: 10.1140/epjad/s2005-04-033-y.
34. H.W. Hammer, U.G. Meissner, D. Drechsel, Phys. Lett. B **367**, 323 (1996).